Available online at www.sciencedirect.com
SciVerse ScienceDirect
Energy Procedia 15 (2012) 248 – 257
Energy Procedia

International Conference on Materials for Advanced Technologies 2011, Symposium O

Improvement of Photodegradation of Silicon Thin-film Solar Cells by pc-Si:H/a-Si:H Multilayers

Yeu-Long Jiang[a,*], Chun-Yen Chen[a], Tai-Chao Kuo[a] and Tuan-Jen Yu[b]

[a]*Institute of Optoelectronic Engineering and Department of Electrical Engineering, National Chung Hsing University, Taichung 402, Taiwan, Republic of China*
[b]*UVAT Technology Co., Ltd, Taichung 428, Taiwan, Republic of China*

Abstract

A series gradual changing of protocrystalline phase of hydrogenated protocrystalline silicon/hydrogenated amorphous silicon (pc-Si:H/a-Si:H) multilayers is fabricated by periodically changing hydrogen dilution ratios ($R = H_2/SiH_4$). Protocrystalline phase can be well identified by Raman peak shift and the variation of dielectric function measured by spectroscopic ellipsometer. Increasing R can effectively increase the protocrystalline phase, optical energy gap, and reduce the density of films. More protocrystalline phase can suppress the photodegradation effects of the pc-Si:H/a-Si:H multilayers solar cells, but reduce the initial efficiency. Therefore, the performance of cells could be optimised by suitable protocrystalline phase for obtaining good stability and efficiency.

Keywords: Solar cells; hydrogenated protocrystalline silicon; hydrogenated amorphous silicon; multilayers; hydrogen dilution; photodegradation

1. Introduction

Hydrogenated protocrystalline silicon (pc-Si:H) film is a promising materials for solar cells, which structure is gradually changed from amorphous phase to the boundary of amorphous and microcrystalline (a + μc) mixed phase along the film growth direction. This gradually changed phase will stimulate the formation of nucleation sites, thus, which is named as protocrystalline phase [1-3]. Due to the incubation of the formation of nucleation sites and the following crystal grain growth, this region of protocrystalline

* Corresponding author. Tel.:+886 4 2284 0688 ext.223; fax: +886 4 2284 1410
E-mail address: yljang@nchu.edu.tw

doi:10.1016/j.egypro.2012.02.029

phase is also called as the incubation layer. In fact, the protocrystalline phase is a gradual changing phase from the amorphous phase of the initial film growth to the microcrystalline phase of the onset of crystal grain nucleation. Increasing hydrogen dilution can reduce the thickness of incubation layer. The gradual changing phase from the amorphous phase to the microcrystalline phase will happen in a thin-thickness region. Some reports show that the pc-Si:H structure can be used to improve the performance of solar cells [4-7]. However, for different hydrogen dilution, the formation of protocrystalline phase in a same fixed thickness within incubation layer is totally different. Therefore, to understand the influence of the pc-Si:H films on the performance of solar cells shall carefully identify the difference of the formation of protocrystalline phase of the films.

In this work, we gradually change the hydrogen dilution ratio ($R = H_2/SiH_4$) to prepare a series of various protocrystalline phase of pc-Si:H films. Since the protocrystalline phase can only exist in the incubation region. In order to maintain the protocrystalline phase, pc-Si:H/a-Si:H multilayers were fabricated, in which 26-nm-thickness pc-Si:H sublayers and 13-nm-thickness a-Si:H sublayers are periodically deposited. The role of a-Si:H sublayers is to interrupt the continuous growth to limit the thickness of pc-Si:H sublayers, thus to maintain the protocrystalline phase [8-10]. The controlling of various protocrystalline phases of pc-Si:H/a-Si:H multilayers is obtained by a series changing of hydrogen dilution ratio R for deposition of pc-Si:H sublayers. The changing of protocrystalline phases of these pc-Si:H/a-Si:H multilayers are analysed by Raman spectrometer and spectroscopic ellipsometer (SE) [11, 12]. The I-V characteristics of the p-i-n solar cells with the i-layer of these pc-Si:H/a-Si:H multilayers are used to identify the influence of the different protocrystalline phase on the performance of solar cells and photodegradation effects.

2. Experimental

2.1. Sample preparation

a-Si:H and pc-Si:H single-layer films, pc-Si:H/a-Si:H multilayers, p-i-n solar cells with i-layer of single-layer of a-Si:H or pc-Si:H, and of pc-Si:H/a-Si:H multilayers were prepared by a single-chamber 13.56 MHz capacitive-type plasma-enhanced chemical vapour deposition (PECVD) system. The substrates used for films and solar cells characterisation were deposited on Corning 1737F glass and Asahi U-type glass, respectively. The substrate temperature, peak RF power and pressure for i-layer deposition were kept at 200^{o}C, 20 W and 1 Torr, respectively. The pc-Si:H/a-Si:H multilayers were deposited with computer control of periodically changing hydrogen dilution ratios ($R = H_2/SiH_4$). The R ratio for pc-Si:H sublayer deposition was changed from 6, 8, 16 and 28 to control the formation of different protocrystalline phase. The R ratio for a-Si:H sublayer deposition was fixed at 4. In order to compare the variation of protocrystalline phase, the thickness of pc-Si:H sublayer is fixed at 26 nm, and that of a-Si:H sublayer is fixed at 13 nm. The total number of layers is 10, and the total i-layer thickness is 390 nm. The thicknesses of p-layer and n-layer are 15 and 30 nm, respectively. The area of the p-i-n solar cells is 7.07×10^{-2} cm^2.

2.2. Sample measurements

Raman spectra were used to characterise the crystal phase change of the a-Si:H and pc-Si:H single-layer films and pc-Si:H/a-Si:H multilayers, which were measured by a spectrometer of NT-MDT MS5400i with 632.8 nm wavelength and 2.27 mW output power. The dielectric function, optical energy band gap were measured and analysed by spectroscopic ellipsometer, which were carried out by a J.A.

Woollam M2000 with the angle of incidence 55° to 70° and the wavelength is from 190 to 1700 nm. The I-V characteristics of solar cells were measured under an ELH lamp illumination with a standard c-Si solar cell calibrated to about one sun condition. In order to control the same light intensity and the uniformity of illumination, the photodegradation rates of different solar cells were measured under the same outdoor sunlight illumination for 45 hours (from A.M. 9:00 to P.M. 3:00 per day). Quantum efficiency (QE) spectra were used to characterize the quantum efficiency of solar cells, which were measured by a TEO QE-3000 with a 150 W Xenon lamp illumination calibrated to about AM 1.5 condition and the wavelength is from 300 to 900 nm.

3. Results and discussion

3.1. Structural properties of a-Si:H and pc-Si:H single-layer films

Figure 1 shows the normalised Raman spectra of the i-layer a-Si:H (or pc-Si:H) films deposited with *R* ratio from 4 to 28, and the Raman peak positions are summarised in Table 1. As *R* ratio is increased from 4 to 28, the Raman Peak at about 482 cm^{-1} of $R = 4$ sample is gradually shifted to 486 cm^{-1} of $R = 28$ sample, indicating that the crystal phase of the film is changed from pure amorphous to protocrystalline. As listed in the Table 1, the Raman peak position of *R* ratio from 4 to 8 is about 482 cm^{-1}, that the crystal phase of these films is pure amorphous. Further increasing *R* ratio from 16 to 28, the Raman peak position is obviously shifted to 484.4 and 485.5 cm^{-1}, respectively. Low *R* ratio less than 8, the crystal structure of the films is mainly amorphous network. High *R* ratio large than 16, the crystal structure of the films contains more protocrystalline phase along the upper portion of film growth direction [13].

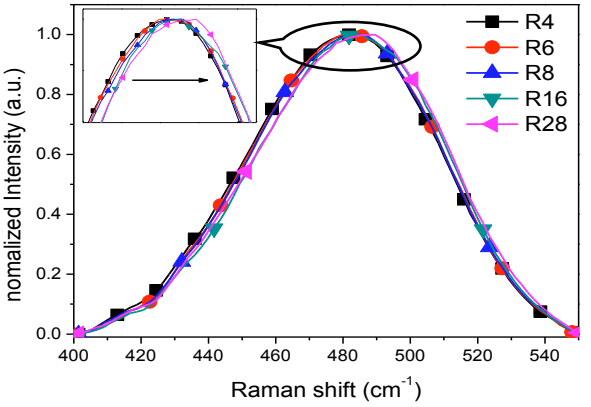

Fig. 1. The Raman spectra of the i-layer a-Si:H (or pc-Si:H) films deposited with *R* ratio from 4 to 28.

Table 1. The Raman peak position of the i-layer a-Si:H (or pc-Si:H) films deposited with *R* ratio from 4 to 28.

R ratio	peak position (cm^{-1})
4	481.7
6	482.0
8	482.5
16	484.4
28	485.5

3.2. Optical properties of a-Si:H and pc-Si:H single-layer films

Figure 2 displays dielectric functions of the i-layer a-Si:H (or pc-Si:H) films deposited with *R* ratio from 4 to 28. The peak position and peak height of dielectric constants of real part (ε_1) and imaginary part (ε_2) are summarised in Table 2. Increasing *R* ratio reduces peak intensity and shifts peak position toward higher energy of ε_1 and ε_2. Cabarrocas *et al.* [14] pointed out that the film with low film density would result in the peak movement of ε_1 and ε_2 toward high-energy and decreasing of the peak height simultaneously. High *R* ratio induces the formation of more protocrystalline phase in the films, which have low film density. As shown in the insets of Fig. 2 and data of Table 2, the lower *R* ratios from 4 to 8 films have similar low-energy peak positions and high peak height of ε_1 at about 2.79 to 2.82 eV and 22.9, and of ε_2 at about 3.66 to 3.70 eV and 25.4 to 25.5. In addition, the higher *R* ratios of 16 to 28 films have high-energy peak positions and low peak height of ε_1 at about 2.83 to 2.87 eV and 22.4 to 21.4, and of ε_2 at about 3.68 to 3.75 eV and 24.9 and 23.8 eV. The results demonstrate that low *R* ratio films exhibit more amorphous phase, and high *R* ratio films contain more protocrystalline phase, resulting in low film density. The reduction of peak intensity at low-energy side of ε_1 and ε_2 corresponds to the low absorption of long-wavelength photons. High-energy peak positions and low peak height of dielectric constants correspond to the Raman peak shifted to high wavenumber.

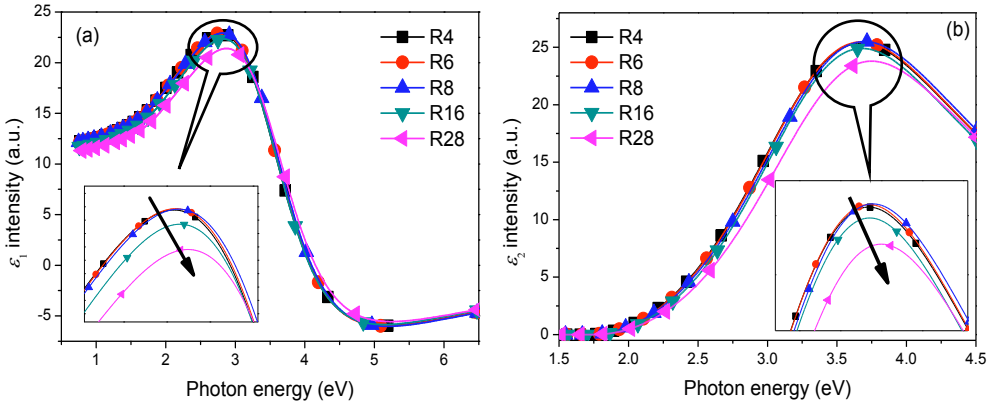

Fig. 2. (a) Real and (b) imaginary parts of the dielectric functions of the i-layer a-Si:H (or pc-Si:H) films deposited with *R* ratio from 4 to 28.

Table 2. The peak position and peak height of ε_1 and ε_2 of the i-layer a-Si:H (or pc-Si:H) films deposited with *R* ratio from 4 to 28.

R ratio	ε_1 Peak position (eV)	ε_1 Peak height	ε_2 Peak position (eV)	ε_2 Peak height
4	2.79	22.88	3.66	25.36
6	2.80	22.93	3.68	25.47
8	2.82	22.91	3.70	25.49
16	2.83	22.35	3.68	24.90
28	2.87	21.40	3.75	23.79

The imaginary part of the dielectric function (ε_2) is analysed by Tauc-Lorentz dispersion law [15], which is expressed as

$$\varepsilon_2 = \frac{AE_nC(E-E_g)^2}{(E^2-E_n^2)^2+C^2E^2}\frac{1}{E}, \quad E > E_g, \tag{1}$$

where A is the amplitude factor proportional to the density of the material, E_n is the peak transition energy, C is the broadening parameter proportional to the degree of disorder of the structure and E_g is the optical band gap. Table 3 summarises these parameters and refractive index at 632.8 nm ($n_{632.8\ nm}$) of the i-layer a-Si:H (or pc-Si:H) films deposited with R ratio from 4 to 28. As the hydrogen dilution ratio increases, the optical energy gap (E_g) increased from 1.69 eV to 1.75 eV, and refractive index ($n_{632.8\ nm}$) decreased from 4.13 to 3.93. High E_n indicates the film containing higher hydrogen content. Therefore, dielectric constant peak position moves to the high energy and the optical energy gap is increased. The lower value of A presents the lower film density and the film contains more internal voids, resulting in decreased refractive index. As shown in Table 3, the films deposited with low R ratios from 4 to 8 exhibit higher A (199.7 to 200.6 eV), lower E_n (3.55 to 3.57 eV), higher C (2.20 to 2.18 eV), lower E_g (1.69 to 1.7 eV) and higher refractive index $n_{632.8\ nm}$ (4.13 to 4.12). Those deposited with high R ratios of 16 and 28 perform lower A (197.4 and 190.6 eV), higher E_n (3.57 and 3.62 eV), lower C (2.18 and 2.17 eV), higher E_g (1.73 and 1.75 eV) and lower refractive index $n_{632.8\ nm}$ (4.03 and 3.93). Increasing R ratio changes the film crystal phase from nearly pure amorphous to more protocrystalline, and result in increasing optical band gap and the order of the structure, but reducing the film density. The results indicate that there are some micro-voids exist in the films.

Table 3. The Tauc-Lorentz dispersion parameters and refractive index of the i-layer a-Si:H (or pc-Si:H) films deposited with R ratio from 4 to 28.

R ratio	A (eV)	E_n (eV)	C (eV)	E_g (eV)	$n_{632.8\ nm}$
4	199.7	3.55	2.20	1.69	4.13
6	201.1	3.55	2.17	1.70	4.13
8	200.6	3.57	2.18	1.70	4.12
16	197.4	3.57	2.18	1.73	4.03
28	190.6	3.62	2.17	1.75	3.93

3.3. Structural properties of pc-Si:H/a-Si:H multilayers

Figure 3 illustrates the Raman spectra of the pc-Si:H/a-Si:H multilayers, and the Raman peak positions are summarised in Table 4. Increasing R ratio for pc-Si:H sublayer deposition from 6 to 28 shifts the Raman Peak at about 481 to 485 cm^{-1}. As shown in Table 4, due to the crystal phase is dominantly amorphous for R6 and R8 sublayers, the peak position of M_R6_R4 and M_R8_R4 multilayers are typical amorphous position at 481 and 481.7 cm^{-1}. For M_R16_R4 and M_R28_R4 multilayers, higher protocrystalline phase existed in R16 and R28 sublayers induces the Raman peak position shifted to high wavenumber of about 484.7 and 484.9 cm^{-1}. The results demonstrate that the degree of protocrystalline structure can be spatially modulated by the pc-Si:H/a-Si:H multilayers with variation of R ratio for pc-Si:H sublayer deposition.

Table 4. The Raman peak position of the pc-Si:H/a-Si:H multilayers.

Sample	peak position (cm^{-1})
M_R6_R4	481.0
M_R8_R4	481.7
M_R16_R4	484.7
M_R28_R4	484.9

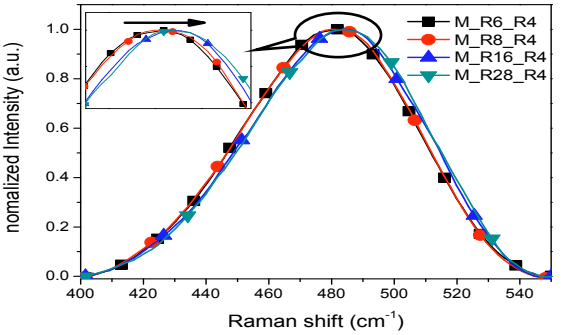

Fig. 3. The Raman spectra of the pc-Si:H/a-Si:H multilayers.

3.4. Optical properties of pc-Si:H/a-Si:H multilayers

Figure 4 displays dielectric functions of the pc-Si:H/a-Si:H multilayers. The peak position and peak height of ε_1 and ε_2 are summarised in Table 5. Increasing R ratio for pc-Si:H sublayer deposition from 6 to 28, the peak position and height of ε_1 and ε_2 are increased from 2.82 to 2.83 eV and decreased from 23.7 to 23.0, and are increased from 3.70 to 3.98 eV and decreased from 26.6 to 24.1. The results further confirm that more protocrystalline phase existed in multilayers will also result in the peak position shifted to high energy and the reduction of peak intensity.

Table 5. The peak position and peak height of ε_1 and ε_2 of the pc-Si:H/a-Si:H multilayers.

Sample	ε_1		ε_2	
	Peak position (eV)	Peak height	Peak position (eV)	Peak height
M_R6_R4	2.82	23.7	3.70	26.6
M_R8_R4	2.81	23.4	3.70	26.1
M_R16_R4	2.82	23.4	3.68	26.1
M_R28_R4	2.83	23.0	3.98	24.1

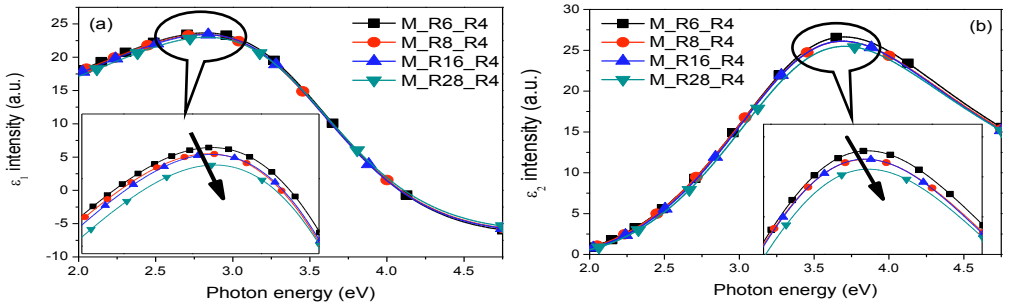

Fig. 4. (a) ε_1 and (b) ε_2 of the pc-Si:H/a-Si:H multilayers.

Table 6 summarises the Tauc-Lorentz dispersion parameters and refractive index at 632.8 nm ($n_{632.8\ nm}$) of the pc-Si:H/a-Si:H multilayers. Increasing R ratio for pc-Si:H sublayer deposition from 6 to 28, the density factor A, the peak transition energy factor E_n, the structural disorder factor C, the optical energy

gap (E_g) and refractive index ($n_{632.8\ nm}$) are decreased from 207.3 to 204.7 eV, fixed at 3.57 eV, decreased from 2.24 to 2.14 eV, increased from 1.68 to 1.73 eV and decreased from 4.20 to 4.10, respectively. More protocrystalline phase existed in multilayers increases the optical energy gap and reduces the density of the multilayers. The variation of protocrystalline phase can be sensitively analysed by Tauc-Lorentz dispersion parameters.

Table 6. The Tauc-Lorentz dispersion parameters and refractive index of the pc-Si:H/a-Si:H multilayers.

Sample	A (eV)	E_n (eV)	C (eV)	E_g (eV)	$n_{632.8\ nm}$
M_R6_R4	207.3	3.57	2.24	1.68	4.20
M_R8_R4	205.7	3.57	2.21	1.69	4.18
M_R16_R4	207.6	3.56	2.17	1.71	4.15
M_R28_R4	204.7	3.57	2.14	1.73	4.10

3.5. I-V properties of the solar cells

Figure 5 demonstrates the I-V curves of the p-i-n solar cells with i-layer of single-layer of a-Si:H or pc-Si:H films (C_R4, C_R6, C_R16, and C_R28), and of pc-Si:H/a-Si:H multilayers (C_M_R6_R4, C_M_R8_R4, C_M_R16_R4 and C_M_R28_R4).

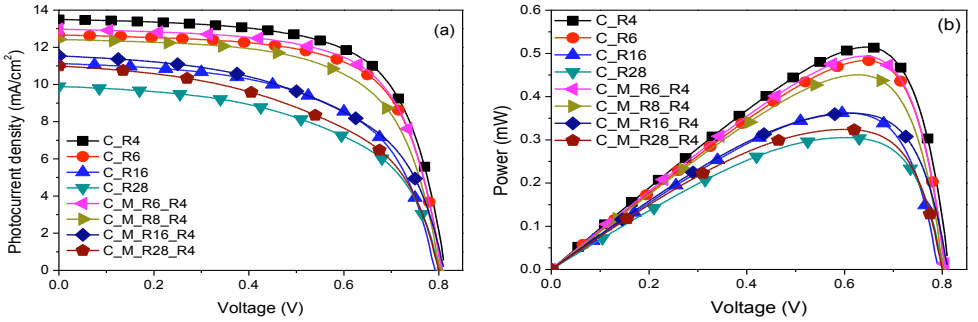

Fig. 5. (a) I-V curves and (b) P-V curves of the solar cells.

Table 7. I-V curves of p-i-n solar cells with i-layer of single-layer of a-Si:H or pc-Si:H films (C_R4, C_R6, C_R16, and C_R28), and of pc-Si:H/a-Si:H multilayers (C_M_R6_R4, C_M_R8_R4, C_M_R16_R4 and C_M_R28_R4).

Sample	V_{oc} (V)	J_{sc} (mA/cm^2)	FF (%)	η (%)
C_R4	0.81	13.5	66.2	7.28
C_R6	0.81	12.7	66.9	6.84
C_R16	0.80	11.1	58.1	5.12
C_R28	0.80	9.9	54.2	4.32
C_M_R6_R4	0.81	13.0	66.8	6.99
C_M_R8_R4	0.80	12.4	63.9	6.38
C_M_R16_R4	0.81	11.5	54.6	5.12
C_M_R28_R4	0.80	11.0	52.1	4.59

Table 7 summarises the open-circuit voltage (V_{OC}), short-circuit current density (J_{SC}), fill factor (FF) and the energy transfer efficiency (η) of these cells. In general, increasing R for both single and multi-layer i-layer cells deposition reduces the values of I_{SC}, FF, and η. High optical energy gap and low film density of more protocrystalline structure result in low I_{SC}, FF, and η. As the protocrystalline phase of

i-layer is increased, there are accompanied the formation of many micro-voids in the films, which reduces the film density. These micro-voids defect centres recombine photo-generated carriers to lower I_{SC}, *FF*, and η. For single i-layer cells, better cells qualities are obtained with lower *R* (4 and 6), the cells have higher *FF* of above 60% and higher J_{SC}, leading to the higher efficiencies of 7.28 and 6.84%. By contrast, for higher *R* (16 and 28), cells have low qualities including lower fill factor of less than 60% and lower J_{SC}, leading to lower efficiencies of 5.12 and 4.32%. For pc-Si:H/a-Si:H multilayers i-layer cells, lower *R* (6 and 8) for pc-Si:H sublayers deposition has also higher *FF* over 60%, higher J_{SC} and efficiencies of 6.99 and 6.38%. By contrast, higher *R* (16 and 28) for pc-Si:H sublayers deposition, cells has also the low qualities including lower *FF* of less than 60% and lower J_{SC}, leading to lower efficiencies of 5.12 and 4.59%. These results illustrate that more protocrystalline phase is unfavourable for collection of photo-generated carriers. High defect densities increase the recombination of carriers, thus the J_{SC} and *FF* are significantly reduced. It is noted that lower performance of single pc-Si:H i-layer cell (C_R16 and C_R28) can be improved by using pc-Si:H/a-Si:H multilayers as the i-layer (C_M_R16_R4 and C_M_R28_R4).

3.6. Photodegradation properties of the solar cells

Figure 6 presents the quantum efficiency (QE) curves before and after photodegradation of single i-layer solar cells. The difference of QE between before and after photodegradation is at the long-wavelength region from 500 to 700 nm. The photodegradation effect is mainly due to the recombination of carriers generated by long-wavelength photons. Notably, for low R4 and high R28 cells, the degradation of QE is more serious than that of the cells of middle R6 and R16. Since the QE is measured under short-circuit condition, the degradation of QE is corresponding the degradation of J_{SC}. The results indicate that there is an optimised protocrystalline structure for reducing the degradation of J_{SC}.

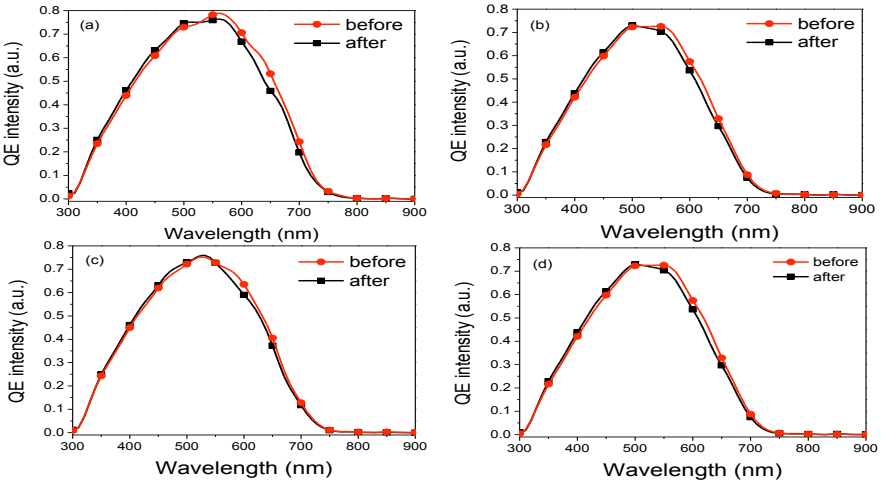

Fig. 6. The QE curves of (a) C_R4, (b) C_R6, (c) C_R16 and (d) C_R28 solar cells before and after photodegradation.

Figure 7 shows the QE curves before and after photodegradation of pc-Si:H/a-Si:H multilayers i-layer solar cells. The difference of QE between before and after photodegradation is also at the long-wavelength region from 500 to 700 nm. For cells with low R6 and high R28 pc-Si:H sublayers, the degradation of QE is more serious than that of the cells with middle R8 and R16 pc-Si:H sublayers. In this work, the optimised protocrystalline structure for reducing the degradation of J_{SC} is C_M_R8_R4.

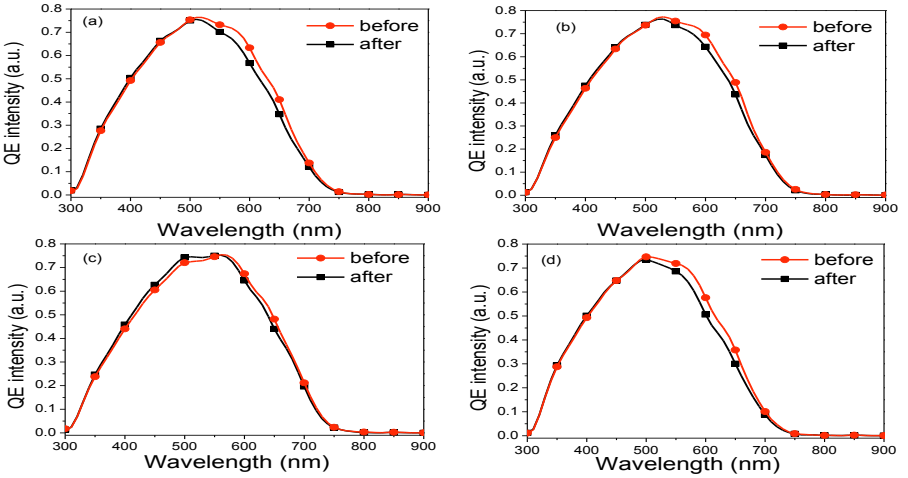

Fig. 7. The QE curves of (a) C_M_R6_R4; (b) C_M_R8_R4; (c) C_M_R16_R4 and (d) C_M_R28_R4 solar cells before and after photodegradation.

Table 8. The photodegradation rates of η, *FF*, J_{SC}, and V_{OC} of the solar cells.

Sample	Photodegradation rate (%)			
	η	*FF*	J_{sc}	V_{oc}
C_R4	22.8	14.3	10.0	0
C_R6	18.0	12.2	7.1	0
C_R16	12.0	4.4	9.7	0
C_R28	9.7	2.0	10.1	0
C_M_R6_R4	18.0	11.2	8.0	0
C_M_R8_R4	13.9	8.4	7.3	0
C_M_R16_R4	10.4	0.9	12.1	0
C_M_R28_R4	8.4	0.2	13.3	0

Table 8 summarises the photodegradation rates of η, *FF*, J_{SC}, and V_{OC} of the cells. In general, increasing *R* ratio to increase protocrystalline structure reduces the photodegradation rate of η and *FF*, and no photodegradation of V_{OC}. Low photodegradation of J_{SC} could be obtained for middle *R* ratio deposition films. Comparison with the data shown in Table 7, the cells with low protocrystalline phase have the initial *FF* higher than 60%, which have high photodegradation rates of η and *FF*. On the contrary, those cells with high protocrystalline phase have the initial *FF* lower than 60%, which have low photodegradation rates of η and *FF*. The cells with high protocrystalline phase already have many defects to recombine the carriers, thus the initial *FF* is low. There is no significant effect on photodegradation by the new generation of defects due to light illumination. From the photodegradation rates of η shown in Table 8, the cells using pc-Si:H/a-Si:H multilayers as i-layer can obtain lower photodegradation rate than those using single-layer pc-Si:H i-layer. Increasing *R* from 6 to 28 could suppress the photodegradation of efficiency (η) of the pc-Si:H/a-Si:H multilayers solar cells from about 18% to 8.4%. However, increasing *R* also reduces the initial efficiency from 6.99% to 4.59%. The amount of protocrystalline phase in pc-Si:H/a-Si:H multilayers can be gradually increased by increasing *R* ratio, and the photodegradation rate is also gradually reduced. Since high protocrystalline phase will reduce the initial efficiency. The optimised performance of pc-Si:H/a-Si:H multilayers solar cells shall be controlled by suitable protocrystalline phase.

4. Conclusions

The gradual change the amount of protocrystalline phase could be well controlled by the pc-Si:H/ a-Si:H multilayers. The Raman spectra and dielectric function and optical properties measured by spectroscopic ellipsometer can sensitively identify the variation of protocrystalline phase of the films. Increasing *R* ratio can obtain more protocrystalline structure in the films with high optical energy gap and low film density, which results in low photodegradation rate but low initial energy efficiency. Therefore, the optimised performance of pc-Si:H/a-Si:H multilayers solar cells for obtaining good stability and efficiency shall be controlled by suitable protocrystalline phase.

Acknowledgements

This work was partially supported by the Central Taiwan Science Park Administration, Taiwan, through grant 301200701.

References

[1] Koval RJ, Pearce JM, Ferlauto AS, Collins RW, Wronski CR. The role of phase transitions between amorphous and microcrystalline silicon on the performance of protocrystalline Si:H solar cells. *Proc. 28th IEEE Photovoltaic Specialists Conf., Anchorage, Alaska;* 2000,750-3.

[2] Collins RW, Ferreira GM, Ferlauto AS, Koval RJ, Pearce JM, Wronski CR, Al-Jassim MM, Jones KM. Thickness evolution of the microstructure of Si:H films in the amorphous-to-microcrystalline phase transition region. *Proc. 3rd World Conf. on Photovoltaic Energy Conversion, Osaka, Japan;* 2003; p.2767-72.

[3] Ferlauto AS, Ferreira GM, Koval RJ, Pearce JM, Wronski CR, Collins RW, AI-Jassim MM, Jones KM. Evaluation of compositional depth profiles in mixed phase (amorphous + crystalline) silicon films from real time spectroscopic ellipsometry. *Thin Solid Films* 2004; **455-456**:665-9.

[4] Koval RJ, Koh J, Lu Z, Jiao L, Collins RW, Wronski CR. Performance and stability of Si:H *p-i-n* solar cells with *i* layers prepared at the thickness-dependent amorphous-to-microcrystalline phase boundary. *Appl. Phys. Lett*. 1999; **75**:1553-5.

[5] Collins RW, Ferlauto AS, Ferreira GM, Chen C, Koh J, Koval RJ, Lee Y, Pearce JM, Wronski CR. Evolution of micro-structure and phase in amorphous, protocrystalline, and microcrystalline silicon studied by real-time spectroscopic ellipsometry. *Sol. Energy Mater. Sol. Cells* 2003; **78**:143-80.

[6] Ahn JY, Lim KS. Amorphous silicon solar cells with stable protocrystalline silicon and unstable microcrystalline silicon at the onset of a microcrystalline regime as i-layers. *J. Non-Cryst. Solids* 2005; **351**:748-53.

[7] Myong SY, Kwon SW, Lim KS, Kondo M, Konagai M. Inclusion of nanosized silicon grains in hydrogenated proto-crystalline silicon multilayers and its relation to stability. *Appl. Phys. Lett*. 2006; **88**:083118.

[8] Kwon SW, Kwak J, Myong SY, Lim KS. Characterization of the protocrystalline silicon multilayer. *J. Non-Cryst. Solids* 2006; **352**:1134-7.

[9] Myong SY, Konagai M, Lim KS. Fast and highly stabilized protocrystalline silicon multilayer solar cell. *Proc. 3rd World Conf. on Photovoltaic Energy Conversion, Osaka, Japan;* 2003, p. 1737-40.

[10] Myong SY, Kwon SW, Lim KS, Konagai M. Highly stabilized protocrystalline silicon multilayer solar cell using a silicon-carbide double p-layer structure. *Sol. Energy Mater. Sol. Cells* 2005; **85**:133-40.

[11] Morral AFI, Cabarrocas PRi. Shedding light on the growth of amorphous, polymorphous, protocrystalline and micro-crystalline silicon thin films. *Thin Solid Films* 2001; **383**:161-4.

[12] Morral AFi, Hofmeister H, Cabarrocas PRi. Structure of plasma deposited polymorphous silicon. *J. Non-Cryst. Solids* 2002; **299-302**:284-9.

[13] Wronski CR, Collins RW. Phase engineering of a-Si:H solar cells for optimized performance. *Solar Energy* 2004; **77**:877-85.

[14] Morral AFi, Cabarrocas PRi, Clerc C. Structure and hydrogen content of polymorphous silicon thin films studied by spectroscopic ellipsometry and nuclear measurements. *Phys. Rev. B: Cond. Mat.* 2004; **69**:125307.

[15] Jellison GE, Modine FA. Parameterization of the optical functions of amorphous materials in the interband region. *Appl. Phys. Lett.* 1996; **69**:371-3.